A Tethered Free-Fall Glider to Measure Ocean Turbulence

B. J. W. GREENAN AND N. S. OAKEY

Ocean Sciences Division, Maritimes Region, Fisheries and Oceans Canada, Dartmouth, Nova Scotia, Canada

(Manuscript received 28 August 1997, in final form 17 August 1998)

ABSTRACT

A tethered free-fall microstructure glider, designed to make quasi-horizontal profiles of the ocean mixed layer, was tested at Emerald Bank on the Scotian Shelf in June 1996. The vehicle attained a 4:1 gliding ratio with the angle of attack close to 0°. The glider typically stabilized its pitch and roll within the first 10 s of each flight. The vehicle speed started at 0.55 m s^{-1} and decreased to 0.45 m s^{-1} over the period of a 300-s flight due in part to the increase in drag of the tether cable. Two profiles of microstructure obtained under moderate and very light wind conditions are presented to illustrate the performance of the glider from very near the surface to depth. These profiles demonstrate the advantages of the glider over vertical profilers in exploring the ocean mixed layer under various forcing conditions.

1. Introduction

Instruments used to measure ocean microstructure can generally be categorized as either vertical or horizontal profilers. Over the past three decades, these profiling instruments have provided oceanographers with a substantially improved understanding of mixing and dissipation within the world's oceans. Vertical profiling has been carried out at the Bedford Institute of Oceanography (BIO) during this era using instruments such as OCTUPROBE (Oakey 1977) and EPSONDE (Oakey 1988). The development of a quasi-horizontal profiler based on the EPSONDE instrument design was undertaken in 1993. This design incorporated the EPSONDE profiler as the payload of a tethered free-fall glider and, thus, minimized the development time and project cost. This tethered free-fall glider (EPSONDE-Glider) differs in several ways from other gliding instruments such as SLOCUM (Simonetti 1998) and ALBAC (Kawaguchi et al. 1993). First, SLOCUM and ALBAC are autonomous underwater vehicles (AUVs) that log data internally, while EPSONDE-Glider has a tether–data link enabling it to provide real-time data during a rapid succession of profiles. Second, EPSONDE-Glider is designed to measure ocean microstructure, whereas SLOCUM and ALBAC measure properties such as temperature and conductivity.

Vertical microstructure profiling has demonstrated the intermittency of ocean mixing in time, depth, and intensity (Osborn 1978; Gregg 1980; Oakey 1985). Due to the logistics of vertical profiler deployment, these datasets provide sparse horizontal sampling, which limits the certainty about estimates of mixing and dissipation made with these instruments. In spite of this intermittency, Oakey and Elliott (1982) determined that the integral of dissipation over the mixed layer accounted for about 2% of the energy flux from the atmospheric boundary layer. In addition, the intensity of the dissipation was found to be well correlated with the cube of the wind speed. Another traditional limitation of vertical profilers is the inability to sample the upper 5–8 m of the ocean mixed layer because the instrument probes typically start ~2 m below the ocean surface and the instrument requires a few meters of free fall before it stabilizes. As well, vertical profilers start close to the ship so measurements are not possible near the surface due to the effect of the ship on the surrounding environment. In an attempt to circumvent these limitations, Anis and Moum (1995) used a freely rising profiler to collect vertical microstructure in the upper oceanic boundary layer.

Measurements of the horizontal variability in the rates of kinetic energy dissipation, ε, have been attempted using platforms including towed bodies (Grant et al. 1962; Gargett 1975; Gargett 1976; Osborn and Lueck 1985a; Lueck 1987) and submarines (Gargett 1982; Osborn and Lueck 1985b; Yamazaki et al. 1990; Osborn et al. 1992). At present, several AUVs (Levine and Lueck 1996; Dhanak and Holappa 1996) are being designed and tested for horizontal microstructure profiling. Lueck et al. (1997) have developed an autonomous moored profiler system that provides long time series of microstructure data; this instrument relies upon am-

Corresponding author address: Dr. N. S. Oakey, Ocean Sciences Division, Bedford Institute of Oceanography, P.O. Box 1006, Dartmouth, NS B2Y 4A2, Canada.
E-mail: oakeyn@mar.dfo-mpo.gc.ca

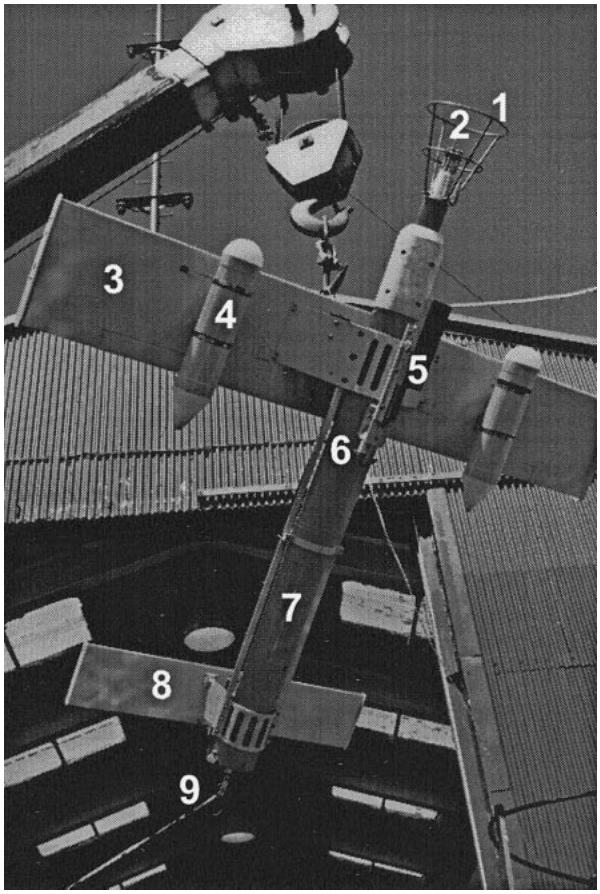

FIG. 1. Photograph of EPSONDE-Glider on the Defence Research Establishment Atlantic barge in Bedford Basin in May 1996 with 1) guard, 2) microstructure sensors, 3) main wing, 4) buoyancy tubes, 5) ballast, 6) release solenoid, 7) EPSONDE pressure case, 8) elevator wing, and 9) tether cable.

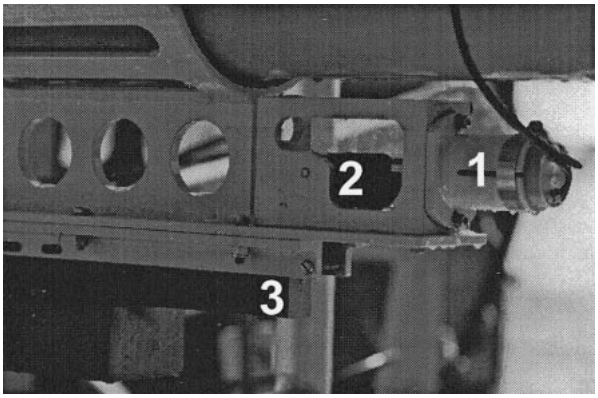

FIG. 2. EPSONDE-Glider ballast release system. Firing the solenoid 1) retracts its cylindrical pin, which, in turn, allows the release mechanism 2) to pivot and drop the ballast weight 3). The ballast weight is attached to the release mechanism via a loop of nylon filament line.

bient currents to advect turbulent eddies past its sensors. Despite these efforts, our knowledge about horizontal variability in the mixed layer remains limited.

The EPSONDE-Glider (Greenan et al. 1997) is a tethered free-fall glider designed for performing quasi-horizontal profiles of temperature microstructure and turbulent shear near the ocean surface. One advantage of this design over towed probes and powered vehicles is that it should be free of the vibrations associated with those methods of propulsion. The data collected using this instrument may allow certain issues to be addressed, such as the averaging required to obtain a suitable estimate of integrated mixed layer dissipation, as well as some insight into intermittency in the ocean mixed layer near the surface.

A series of tests were performed with EPSONDE-Glider on the CSS *Parizeau* from 17–30 June 1996. The experiment site was located at Emerald Bank on the Scotian Shelf in a relatively level area of 100-m-deep water. As a complement to glider tests, the following measurements were also performed: 1) EPSONDE (Oakey 1988) vertical profiles of ocean microstructure, 2) air–sea flux measurements with a bow anemometer system (Dobson et al. 1994), 3) boundary layer meteorological data collected with a Minimet buoy, 4) wave spectra from a Datawell ''Waverider'' buoy, 5) acoustic Doppler current profiler (ADCP) profiles, 6) CTD profiles, and 7) wave measurements using a ship-mounted radar. These results are being prepared for a separate paper and will not be discussed further here.

The design objectives and outcomes of the EPSONDE-Glider are presented in section 2. The instrument performance during the field experiment are discussed in section 3, and a summary is provided in section 4.

2. Instrument design

A tethered free-fall microstructure glider was designed to sample the horizontal and vertical variability of mixing processes along a gradually descending flight path in the ocean mixed layer. The configuration of EPSONDE-Glider is illustrated in Fig. 1. The main wing is mounted above the chassis of the vehicle on four aluminum struts. This wing has a span of 2.43 m and chord of 0.43 m and generates the lift force for the glider. A combination of two main wing ailerons and the elevator wing enable the operator to control the vehicle roll and pitch, respectively. The elevator wing has a span of 1.22 m and chord of 0.25 m and is attached to the vehicle with two upright aluminum plates, which serve as vertical stabilizers (this may be seen better in Figs. 6 and 7). A cylindrical pressure case, 0.16-m diameter, houses the EPSONDE and glider control electronics and serves as a low-noise platform on which the ocean microstructure sensors are mounted. A 12-kg ballast weight provides the motive force for the glider, and an underwater solenoid releases the ballast when necessary (Fig. 2). This ballast release system serves as a

safety system that can be activated in a number of ways. The Pelagic Electronics underwater solenoid used in this system proved to be an extremely reliable device. In the current configuration (Fig. 2), when the solenoid is fired the pin is retracted and this allows a cantilevered release mechanism to rotate due to the weight of the attached ballast. When the release mechanism completes its rotation the nylon monofilament line used to attach the steel ballast slides off of a pin on the front of the release mechanism and detaches itself from the glider. The glider is approximately 7 kg negatively buoyant with the ballast weight attached and, hence, has sufficient buoyancy to surface when the weight is released (positively buoyant by 5 kg). The combined vehicle tether–data link is provided by a four-conductor Kevlar cable (typically 1000 m), which has a weight in water of 1 kg (100 m)$^{-1}$ and a breaking strength of 8000 N (1800 lbs).

Since the EPSONDE-Glider mechanical design goal was to provide a low-noise, high lift-to-drag ratio glider to carry an EPSONDE profiler as its payload, the profiler body is isolated as much as possible from the remainder of the vehicle by using 0.01-m-high performance open-cell urethane foam manufactured by Protech. This foam acts as a spring suspending the pressure case, while the motions of the water in the foam are damped by viscosity (Lueck et al. 1997). The frame of the vehicle was constructed at BIO using corrosion-resistant 6061 T6 aluminum. Slots were milled in various aluminum parts of the frame to keep the overall weight of the vehicle to a minimum. In addition, the slots in the frame, which cradles the profiler, reduce the contact area between the profiler and the frame, with the intent of reducing noise transmission. The buoyancy of the vehicle was also an important factor because, by reducing the amount of aluminum on the vehicle, the amount of syntactic foam mounted on the exterior of the vehicle (or size of buoyancy tubes) could be kept to a minimum, thus reducing the drag of the instrument.

The elevator wing at the rear of the vehicle is a symmetrical airfoil section constructed of molded fiberglass. The main wing is a cambered, fiberglass airfoil (carbon fiber reinforced) provided by Kaiser Compositek. Both the main and rear wing are filled with syntactic foam, which has a density of 520 kg m^{-3}, to increase the buoyancy of the vehicle.

Oceanographic data collected by sensors on the sting of the vehicle include CTD, and temperature and velocity microstructure (Oakey 1988). The CTD signal, which is sampled at 32 Hz, comprises conductivity and temperature from an Ocean Sensors device with depth being provided by a Viatran model 207C1 strain gauge pressure transducer. Temperature microstructure is derived from a Thermometrics FP07 fast thermistor and a DISA platinum thin-film sensor. The thermistor, which has a time constant of ~10 ms, is sampled at 32 Hz with the differentiated signal sampled at 128 Hz. The thin-film sensor, which has a time constant of 2 ms, is sampled at 32 Hz with the differentiated signal sampled at 256 Hz providing a temperature gradient signal. Velocity microstructure is measured using two axisymmetric airfoil shear probes (Osborn and Crawford 1980) constructed at BIO. Turbulent fluctuations produce lift on the probes, and the deflection caused by this force is sensed by a piezoceramic crystal mounted inside the probe tip. The cutoff scale for such devices is ~2 cm. The shear probe signal is sampled at 32 Hz with a differentiated signal sampled at 256 Hz providing a velocity shear estimate. In all cases the time derivative signals are converted to spatial derivatives by making use of the nearly constant instrument speed and Taylor's hypothesis. The electronic signals from the sensors are preconditioned by the electronics in the sting of the EPSONDE3 profiler. These data are then amplified, conditioned, and converted to a digital signal by electronics within the EPSONDE3 main pressure case prior to transmission to an EPSONDE PC deck unit via two wires of the Kevlar cable data link (Oakey 1988).

Flight control is performed by a combination of a Glider control (GC) deck unit and an ONSET Computer Corporation TattleTale Model 8 computer mounted inside the pressure case of the glider. The Model 8 is based on Motorola's MC68332, which is an autonomous, microcoded timing processor designed for control applications. The two computers communicate once per second using an RS-485 telemetry link through two wires of the Kevlar cable. The design and fabrication of the microcontroller circuit board, and associated firmware for the TattleTale 8, was carried out by Satlantic Ltd. When the TattleTale program starts it waits for a configuration command from the deck unit before entering its control mode.

While the TattleTale is in control mode it monitors several parameters related to the orientation and movement of the glider. These include instrument pitch, roll, pitch rate, and roll rate measured by a KVH digital gyro inclinometer. The inclinometer was isolation-mounted inside the pressure case to minimize the effect of its vibration on the microstructure sensors on the sting. Nevertheless, as we will discuss later, the inclinometer appears to be a source of a persistent 10-Hz spike in the data spectra. Heading is recorded by a KVH C100 digital fluxgate compass. A custom-designed impeller-type flowmeter (Fig. 3) mounted on the main wing provides a measure of forward speed. Four magnets mounted on the impeller shaft were used in combination with a Hall-effect sensor to monitor the rotation of the shaft. The results of a calibration of the flowmeter carried out in a linear tow tank at BIO (Fig. 4) indicate a linear relationship between speed and flowmeter output in pulses per second for the range of speeds attained by the glider. To achieve an acceptable flow speed resolution of $\pm 2\%$ in the range of 0.4–0.6 m s^{-1} requires averaging the flowmeter output for at least 5 s or 2 m of flight path. Depth is provided by the EPSONDE3 strain gauge pressure transducer. The TattleTale sends these parameters to the GC deck unit once per second

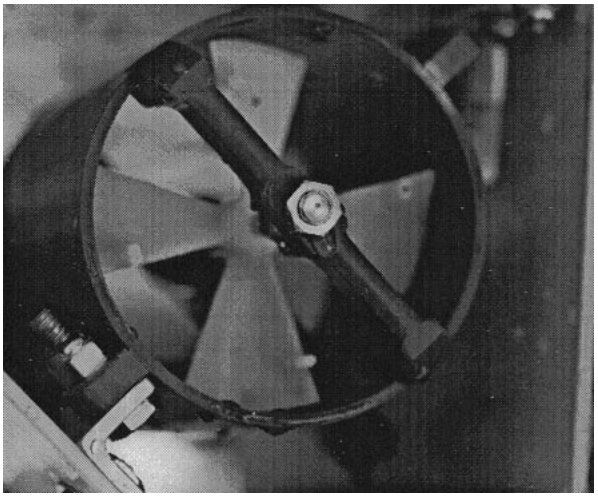

FIG. 3. Impeller-type flowmeter to measure speed of the glider relative to the water. The flowmeter is mounted on a support strut of the main wing. Four magnets are mounted in the shaft of the flowmeter to provide a signal for a Hall-effect sensor mounted in the PVC casing.

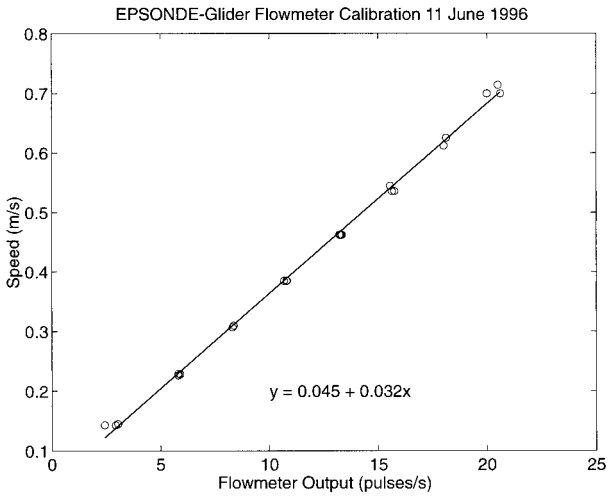

FIG. 4. Calibration results of the EPSONDE-Glider flowmeter in a linear tow tank at BIO. The pulse rate was recorded by the glider control deck unit, and the speed was determined using a stopwatch over an 8-m run. The equation in the figure represents a least squares fit to the data.

and then waits for a response from this PC. The PC program written in Microsoft Visual Basic 3.0 displays the results for the operator (Fig. 5) and logs the data to a file.

The graphical user interface shown in Fig. 5 is divided into two sections: 1) the upper part (dark gray background) provides information to the operator about the glider flight status and 2) the lower part (light gray background) provides buttons that allow access to other windows related to controlling the glider. The gauge in the upper-left corner is similar to an aircraft altimeter and displays the depth of the glider as determined by the onboard pressure transducer. The speed gauge provides the relative speed of the glider in the water as determined by the flowmeter. The heading gauge provides the heading of the glider from the KVH C100 compass. The artificial horizon gauge integrates the pitch and roll signals from the KVH digital gyro inclinometer. Pitch, pitch rate, roll, and roll rate are also displayed in text boxes on the right of the artificial horizon gauge. Below these text boxes an autopilot LED indicates whether the glider control program is in a manual control mode (LED is gray) or in an autopilot mode (LED is red). Below the heading gauge a mode text box indicates the mode of the TattleTale microcontroller on board the glider (configuration, remote, recover). A message text box is used to display any messages the microcontroller sends to the GC deck unit and the data string text box shows the microcontroller data string transmitted once per second. The errors and total strings text boxes monitor the quality of the controller data signal. Some difficulties were originally encountered with cross talk in the four-wire tether cable, which transmitted both the controller and EPSONDE data streams; however, this was eliminated by appropriate cable termination so that both the EPSONDE and the glider control signal were essentially error free.

The glider has been designed such that the TattleTale can govern 1) a servo-controlled elevator wing with the intent of changing the pitch of the glider (Fig. 6); 2) two servo-controlled main-wing ailerons, which work in tandem (180° out of phase) to adjust the roll; and 3) an underwater solenoid, which releases the 12-kg ballast weight (Fig. 2). The GC deck unit operator can either choose to change elevator and/or aileron position by sending a command to the TattleTale or choose to set the GC deck unit program in an autopilot mode. Autopilot is simply a feedback loop in the deck unit program that attempts to fly the glider at a predetermined pitch; data collected from the inclinometer over the previous 5 s of flight is used to determine the necessary adjustment of the elevator wing. If the TattleTale loses communication with the deck unit for a specified amount of time or if the glider goes below a preset maximum depth, the TattleTale computer fires the solenoid, which releases the ballast and the glider returns to the surface. The GC deck unit operator can also send a command to the microcontroller to release the ballast, if necessary. If for some reason the solenoid release system does not work, the ballast is attached to the glider body with a galvanic release, which decays over the period of 1 day.

To ensure that the center of buoyancy of EPSONDE-Glider was located underneath the center of lift for the main wing, ballasting tests were performed in the marina at BIO. In addition, the buoyancy of each component of the vehicle was determined in a freshwater tank at BIO (see Table 1). The steel ballast weights were produced using two lengths of dimensions $1'' \times 3'' \times 12''$ and $2'' \times 3'' \times 12''$, which were welded together in a design that maintained the center of buoyancy under the

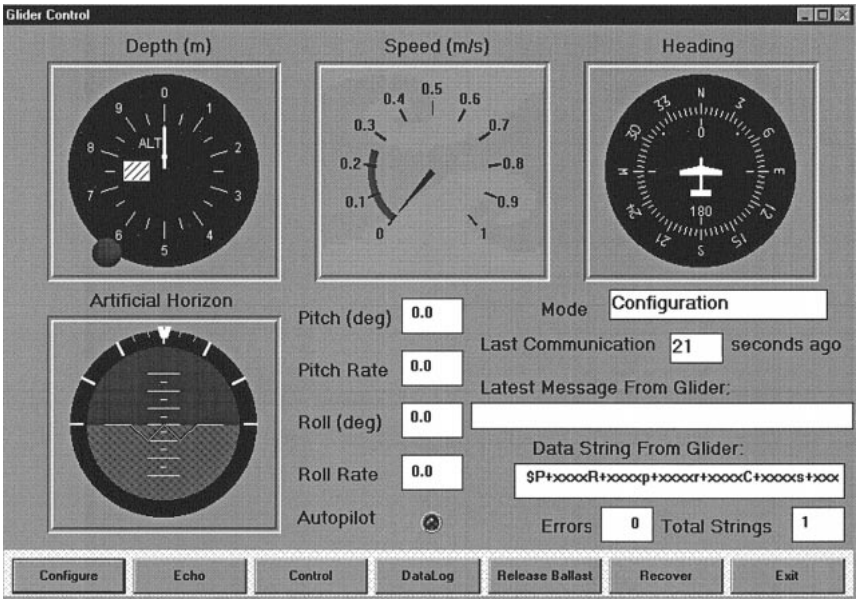

FIG. 5. Glider control deck unit graphical user interface. Current status is displayed on the gauges. Buttons along bottom control various aspects of flight.

center of lift as well as minimized the side load on the release pin of the underwater solenoid. In Fig. 7 the angle of attack and the gliding angle of the vehicle are represented by α and β, respectively. The angle of attack represents the angle between the centerline of the vehicle and the flight path or freestream velocity. The gliding angle is the angle between the horizontal plane and the flight path. The maximum velocity such a glider can attain during a dive is a function of its drag characteristics and weight (Dommasch et al. 1967). The vertical component of the forces are given by

$$W - \frac{1}{2}\rho V^2 A C_L \cos\beta - \frac{1}{2}\rho V^2 A C_D \sin\beta = 0, \quad (1)$$

where W is the weight in water, A is the area, and C_L and C_D are the lift and drag coefficients for the instrument, respectively. Here C_L and C_D represent the sum of the components of the glider, which includes the main wing, tail (elevator) wing, body, and tether cable. The horizontal component is given by

$$C_L \sin\beta - C_D \cos\beta = 0. \quad (2)$$

It is evident from (2) that the gliding angle of the instrument, β, is completely determined by the lift-to-drag ratio of the glider. The lift and drag coefficients for the Compositek wing profile (main wing) were computed by Chris Williams at the Institute for Marine Dynamics (National Research Council of Canada, St. John's, Newfoundland) and are summarized in Table 2. Substituting the appropriate lift and drag coefficients (see section 3b) for the various parts of the glider, the expected gliding angle is approximately 10°, which translates to a ratio of 5.7:1.

The angle of attack, α, may be estimated from the moment equation, which is expressed as

$$-l_W W \cos(\beta - \alpha) + l_{\text{wing}} L_{\text{wing}} \cos(\alpha) + l_{\text{wing}} D_{\text{wing}} \sin(\alpha) + l_{\text{tail}} L_{\text{tail}} \cos(\alpha) + l_{\text{tail}} D_{\text{tail}} \sin(\alpha) + l_{\text{body}} L_{\text{body}} \cos(\alpha) + l_{\text{body}} D_{\text{body}} \sin(\alpha) = 0, \quad (3)$$

where l_w is the distance of the center of gravity from the body apex; and l_{wing}, l_{tail}, and l_{body} are the distances from the body apex to the aerodynamic centers of the main wing, tail, and body, respectively. Here L_{wing}, L_{tail}, and L_{body} represent the lift forces of the wing, tail, and body, respectively, while D_{wing}, D_{tail}, and D_{body} represent the drag forces. This equation assumes that the tether cable has a minimal effect on the static stability of the glider (i.e., the tension from the cable is along the instrument axis). Based on the performance of the vehicle over the distances tested, this seems to be a valid assumption because the flight pitch and roll do not change substantially over the course of a profile. We are unable to quantify this assumption because we can only speculate on the cable catenary as it falls through the water while at the same time being pulled by the glider. This lack of knowledge about the cable also adds uncertainty to estimate the total drag of the glider system. Empirical formulations do exist to estimate cable drag of towed bodies in water. However, this tethered free-glider scenario differs from those because the cable is paid out into the water at a rate faster than the descent rate of the glider. The cable is slightly negatively buoyant in water [$\sim$1 kg (100 m^{-1})] and, therefore, sinks as the glider pulls on it. Hence it is difficult to estimate the exact path the cable follows through the water. This

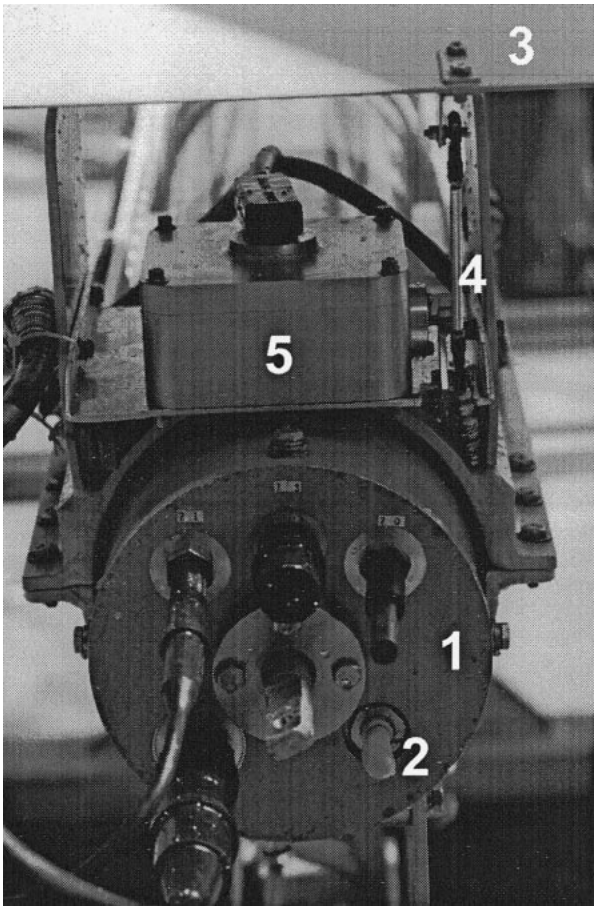

FIG. 6. Photograph of the EPSONDE-Glider end cap 1) with various Electro–Oceanics connectors for data signals and power as well as a bladder 2) for the strain gauge pressure sensor. The angle of the elevator wing 3) is controlled by a connecting arm 4) that is attached to a servo mounted in a pressure-sealed case 5).

TABLE 1. Buoyancy of the various components of EPSONDE-Glider based on measurements carried out in a freshwater tank at BIO.

Glider part description	Buoyancy (kg)
Main wing	+4.68
Rear wing	+1.26
EPSONDE3 payload (rear light by 1.49 kg and front heavy by 2.51 kg with respect to center of buoyancy)	−1.02
Syntactic foam on EPSONDE3 sting	+2.30
Servo case for rear wing	−0.98
Buoyancy tubes on main wing (2 at 3.227)	+6.45
Angle frame and rear aluminum struts	−4.37
Solenoid	−0.76
Aluminum main wing struts, solenoid case, and ballast mount	−2.83
Total	+4.73

makes it difficult to determine the appropriate drag coefficient based on either the cross-sectional or tangential drag. The change in flight performance at the beginning and end of a profile could be used to estimate cable drag, but this would necessitate some knowledge about what fraction of the cable paid out was actually being towed by the glider. The use of a tether cable, which is closer to neutral buoyancy, would simplify this problem.

3. Instrument performance

a. Deployment and recovery

EPSONDE-Glider was deployed from the stern of the CSS *Parizeau* using the stern crane attached to a lift point on the main wing. The glider was lowered into the water and the crane attachment was released. An example of this procedure is shown in Fig. 1 during tests on the Defence Research Establishment Atlantic barge in Bedford Basin. At the start of a descent the glider is pulled back to within 20–30 m from the ship and momentarily rests flat on the surface of the water. When the Kevlar tether cable is released by the deck operator the nose of the glider begins to sink. When this happens circulation begins around the main wing and lift is produced. As the vehicle starts to glide away from the ship, cable is paid out using a specialized winch–capstan handling system. The deck operator uses the capstan to feed out the cable so that the tether line

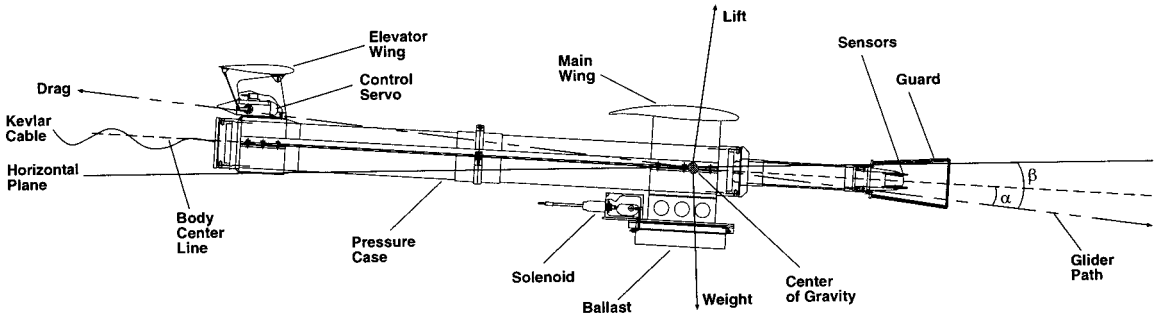

FIG. 7. Side-view schematic of the EPSONDE-Glider. Shear and temperature microstructure measurements are made by sensors on the sting. Data are processed by electronics housed in a pressure case and are transmitted to the ship via the Kevlar cable data link. Glider pitch is controlled via a servo on the elevator wing. Servo-controlled ailerons on the main wing (not shown) adjust roll. The underwater solenoid releases the ballast weight as necessary.

TABLE 2. Summary of calculated lift and drag coefficients for Compositek wing profile (main wing) at various angles of attack.

Angle of attack (α)	Lift coefficient (C_L)	Drag coefficient (C_D)	C_L/C_D
0	0.433	0.0275	15.7
4	0.672	0.0549	12.2
8	0.969	0.1173	8.3
10	1.093	0.1486	7.4
12	1.185	0.1762	6.7
16	1.256	0.2161	5.8

remains loose. At the end of a run the cable is removed from the capstan and the winch is used to pull the glider back to the ship using a sheave block in the stern A-frame. When the glider returns to the surface several tens of meters from the ship, the capstan is reloaded and the procedure is repeated. By keeping the glider as far from the ship as reasonable at the start of a profile, disturbances due to the ship's wake were minimized as much as possible. During recovery the glider is brought up to the rail using the tether cable and winch. The crane is then attached to the lift point on the main wing and the glider is brought in board and placed on its work stand.

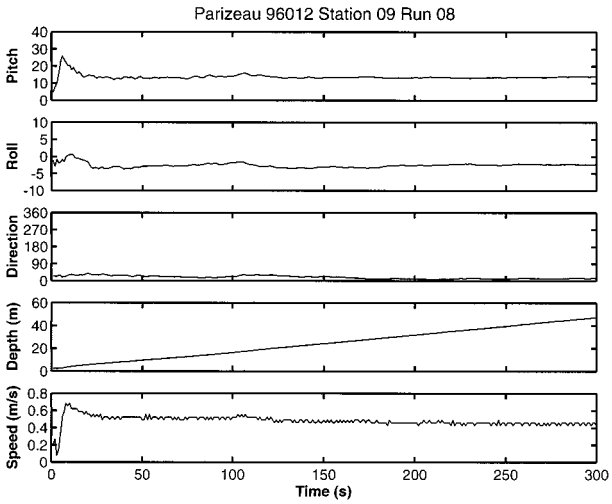

FIG. 8. Parameters measured by EPSONDE-Glider during descent. The initial jump in the pitch signal occurs as the nose of the glider sinks before the main wing generates substantial lift. Increase in depth is almost linear. Speed decreases slightly over the course of flight due to increased drag of tether cable. Noise in the speed signal is due to the limited resolution of the impeller system, which only produces four electronic pulses per revolution.

b. Flight performance

The normal operating procedure for tethered free-fall instruments is to allow the ship to drift with the wind, with the instrument deployed in a direction such that the ship and glider separate and the ship does not overrun the loose cable. With the predominance of light winds on the Scotian Shelf during the cruise, the ship tended to drift more with the surface current than with the wind. This made it difficult to find appropriate conditions for deploying the glider so that proper separation between the glider and ship were attained during each run. In addition, the glider instrumentation gave no measure of lateral glider movement caused by ocean currents and, hence, it was difficult to compensate for this.

An attempt was made to test the glider off the stern with the ship at anchor with the head into the wind. In this situation under moderate winds of 6 m s^{-1} glider trials worked well. However, high seas eventually forced the ship to pull anchor. The results from one of the runs is shown in Fig. 8 for station 9 run 8. At the start of the run, the glider inclinometer indicates the vehicle rests horizontally at the surface. There is an $\sim 2°$ offset in the roll due to alignment differences between the inclinometer and the vehicle body. When the glider tether is released the nose of the glider sinks below the surface and the pitch increases to 25°. Within 10 s the vehicle levels out to a very stable pitch of $14° \pm 1°$ and remains at this angle until the end of the run. The inclinometer roll indicates the instrument remains level throughout the flight and the compass heading remains almost constant. The power spectrum of the pitch and roll signals did not display any significant low-frequency peaks. Most of the variations in these signals seem to be related to the local physical conditions. For example, in Fig. 8 the pitch of the instrument peaks at $\sim 16°$ at about 100 s at the base of the mixed layer where there is larger shear. The depth recorded by the pressure transducer increases linearly with time. The vehicle speed initially peaks around 0.6 m s^{-1} at the start of the run and then quickly settles to 0.55 m s^{-1}. Toward the end of the flight, the glider speed is reduced to 0.45 m s^{-1}, which we attribute to increased drag of the tether.

Using the speed and depth results from station 9 run 8, it is apparent that the actual glider path is a 4:1 (angle between flight path and horizontal plane of 14°) ratio of horizontal to vertical distance traveled during the first part of the run. As more cable is continually added to the system the total drag increases to the point where the ratio is reduced to 3:1 (angle between flight path and horizontal plane of 18°) at the end of a 300-s flight. Hence, for the first part of the run the glide path and vehicle pitch are the same (i.e., the angle of attack is 0°). In a series of runs at a previous station the elevator angle was adjusted to test the affect on the glider flight. It was found that while shifting the elevator could change the pitch over a range of 7°–20°, at lower angles of attack the gliding path remained close to 14°. A number of attempts were made to reduce the drag of the instrument. Nevertheless, the 4:1 gliding ratio was not improved substantially. Hence it was decided to set the elevator so that the angle of attack, α, would be close to zero.

Data collected with the ship drifting on a day with very light winds are displayed in Fig. 9. Results are very similar to those in Fig. 8 with the exception that

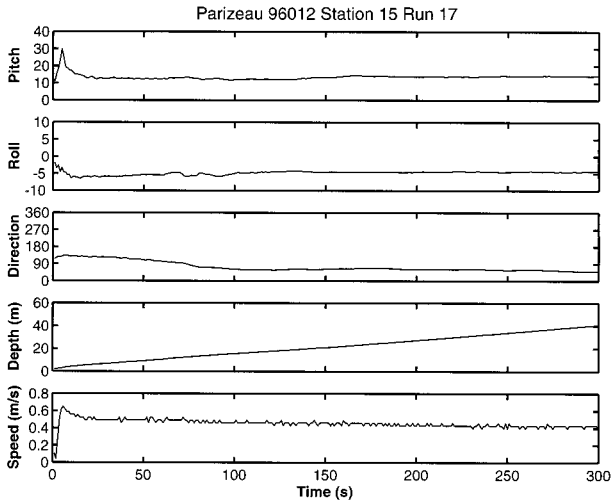

FIG. 9. Results during flight on a calm day are very similar to those in Fig. 8. However, in this case there is a slight roll to the vehicle during most of the run.

there was a slight roll of ~5° at the start of the run, which caused the glider to change direction by ~90° during the course of the run. The reason for this roll is probably due to some initial condition at the surface.

If we consider the forces perpendicular to the glider path, the lift of the main wing may be expressed as

$$\text{lift} = \frac{1}{2}\rho V^2 C_L A_{\text{wing}}, \tag{4}$$

where ρ is the water density (1000 kg m^{-3}), V is the glider speed (0.5 m s^{-1}), and A_{wing} is the wing planform area (1.07 m^2). The component of weight in this direction is equivalent to $W_1 = W\cos(\beta)$, where W is the weight in water of the glider and β is the glide angle. If we assume the glide angle is 14°, then based on the 7-kg negative buoyancy of glider $W_1 = 69.1$ N. The calculations of lift for various angles of attack are summarized in Table 3, with a lift force of 57.5 N at a zero angle of attack. A conservative estimate of lift produced by the elevator wing indicates it would be at most 2 N. Hence the results of this calculation imply an angle of attack of ~2° would provide a match of the weight component and lift force.

The component of weight in the direction of the glider path is equivalent to $W_2 = W\sin(\beta) = 17.2$ N. For a speed of 0.5 m s^{-1} the dynamic pressure ($\frac{1}{2}\rho V^2$) is equal to 125 Pa, and the drag force is calculated by

$$\text{drag} = \frac{1}{2}\rho V^2 A C_D, \tag{5}$$

where A is the area and C_D is the drag coefficient (the drag coefficients for the wings are based on planform area, whereas the drag coefficients of the remaining components of the glider will be based upon projected frontal area). The main wing drag coefficient is given in Table 2 and the area is 1.07 m^2. The elevator wing drag coefficient is assumed to be 0.2 (because the wing tends to be set ~20° off the gliding plane) and area is 0.1 m^2. The body diameter with the aluminum casing for wing mount is estimated to be 0.18 m, and the drag coefficient for the body is assumed to be 0.4. The solenoid plus drop weight frontal area is ~0.01 m^2 and has a drag coefficient of 1.2. The frontal area of the wingtip buoyancy is ~0.008 m^2, and the drag coefficient is estimated to be 0.5. Table 4 summarizes the drag force acting on EPSONDE-Glider for various angles of attack with the simplifying assumption that drag for components other than the main wing does not change substantially over the range of attack angles listed. It is evident from Table 4 that the estimates of drag in the 0°–4° range of attack angles is smaller than the weight component in this direction. One possible explanation for this discrepancy is that the main wing may not be as efficient as estimated due to mounting straps and lifting point brackets mounted on its surface. This explanation appears to be confirmed by recent (July 1998) tests of the instrument in Bedford Basin after considerable effort had been expended to streamline the main wing. After these revisions the instrument achieved an improved glide ratio.

TABLE 3. Summary of lift produced by main wing EPSONDE-Glider at various angles of attack.

Angle of attack (α)	Main wing lift (N)
0	57.5
4	89.2
8	129
10	145
12	157
16	168

c. Temperature and velocity microstructure

The glider payload consisted mainly of the EPSONDE3 microstructure profiler (Oakey 1988), which measures temperature and velocity microstructure. Results from this part of the instrument are displayed for the case of moderate winds in Fig. 10. The shear probes provide measures of variance in the velocity signal in both the vertical and horizontal directions, ∂SH_1 and ∂SH_2, respectively. Time derivatives of the signals are shown but are converted to spatial derivatives using the nearly constant instrument drop speed and Taylor's hy-

TABLE 4. Summary of drag force acting on EPSONDE-Glider for various angles of attack.

Angle of attack (α)	Main wing drag (N)	Total drag (N)
0	3.75	9.5
4	7.36	13.1
8	15.7	21.5
10	19.9	25.7
12	23.6	29.4
16	28.9	34.7

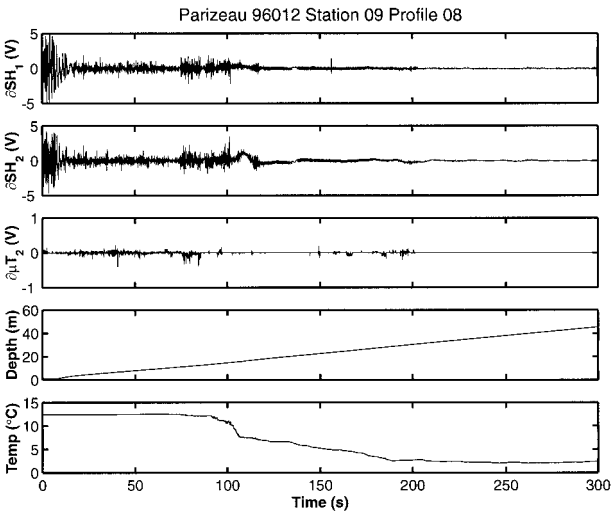

FIG. 10. Temperature and velocity microstructure for the case of moderate winds. Gradients in vertical and horizontal shear (∂SH_1 and ∂SH_2, respectively) and temperature ($\partial \mu T_2$) indicate strong mixing throughout the oceanic mixed layer.

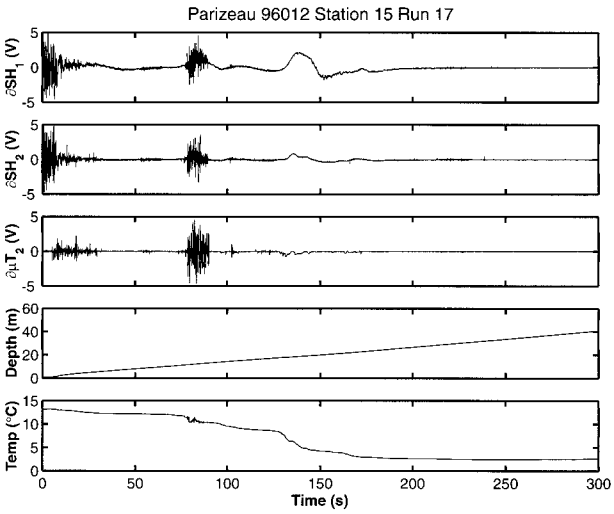

FIG. 11. Temperature and velocity microstructure under very light wind conditions indicate very little mixing except in a small region centered at 12 m.

pothesis. The top two panels of Fig. 10 demonstrate fairly isotropic conditions throughout the mixed layer, which extends to approximately 12 m. The variance in shear is very large at the surface (at time zero) as the glider is being held by the tether. Within a few seconds after the glider is released, the microstructure and turbulent shear signals are free of surface-induced noise, indicating that the instrument is able to provide data within 2–3 m of the surface. The kinetic energy dissipation, ε, increases from $\sim 2 \times 10^{-7}$ W kg^{-1} throughout the upper mixed layer to 1×10^{-6} W kg^{-1} at the base. The signal then decreases to the order of 10^{-9} W kg^{-1}, which appears to be approximately the noise level of the instrument (for comparison, the noise level of the EPSONDE vertical profiler is $\sim 2 \times 10^{-10}$ W kg^{-1}). Analysis of spectra from the flight indicates that some noise spikes do exist at low frequencies that must be removed. The gradient in the temperature signal, $\partial \mu T_2$, (panel 3 of Fig. 10) indicates strong mixing occurring throughout the mixed layer as well as a few isolated events at depths between 20 and 40 m.

The microstructure data recorded at station 15 run 17 is shown in Fig. 11. The winds were very light on this day as is evident in the ∂SH_1, ∂SH_2, and $\partial \mu T_2$ signals throughout the mixed layer. Very little mixing occurs above and below a small region of activity centered at 12 m. In this active mixing region there is a large step in temperature and the gradient $\partial \mu T_2$ is significantly enhanced. There is also a correlation in the velocity shear signals with values of ε to 5×10^{-7} W kg^{-1} in this active region. Changes in the instrument electronic settings between stations 9 and 15 improved the shear measurements by significantly reducing high-frequency noise.

Spikes in the spectra create a problem in estimating the correct variance and hence the correct dissipation. Therefore, an important consideration for a new platform for turbulence measurement is the level of vibrational noise transmitted to the location of the sensors. This might be addressed by positioning accelerometers near the sensors, but this was not done. A composite spectrum of three realizations during a flight with dissipation ranging from $\varepsilon = 9 \times 10^{-7}$ W kg^{-1} to $\varepsilon = 9 \times 10^{-10}$ W kg^{-1} is shown in Fig. 12. These spectra have been corrected for all sensor and electronic transfer functions, and there is in general good agreement between data and corresponding universal form. The highest dissipation regions characterized by the most ener-

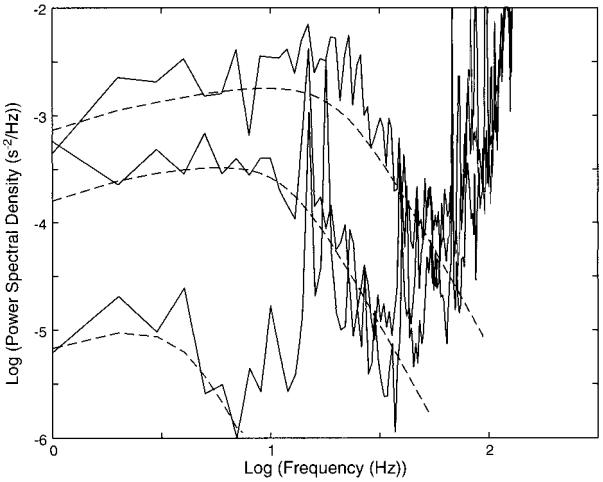

FIG. 12. A composite spectrum from ∂SH_2 for station 9 run 9 is shown for dissipations, ε, of $\varepsilon = 9 \times 10^{-10}$ W kg^{-1}, $\varepsilon = 9 \times 10^{-8}$ W kg^{-1}, and $\varepsilon = 9 \times 10^{-7}$ W kg^{-1}. The spectra are plotted as solid lines and the corresponding universal curves are dashed. This illustrates where vibrational frequencies in the instrument are problematic.

getic curve are not seriously affected by noise spikes; however, at $\varepsilon = 9 \times 10^{-8}$ W kg^{-1} two spikes near 25 Hz require correction. For the smallest dissipation shown $\varepsilon = 9 \times 10^{-10}$ W kg^{-1}, an additional small peak at about 10 Hz is apparent. Most of the problems of spikes in the data shown can be handled quite effectively by careful analysis. Reducing these spikes has been the focus of recent instrument improvements, such as very careful fairing of projecting surfaces, and tests were carried out in July 1998 in Bedford Basin. Although spectra are not shown here for comparison, in general the spectral noise spikes have been reduced and in particular the most troublesome spike at 10 Hz, which limits the low dissipation measurements, has been found to be associated with the gyro-stabilized pitch–roll sensor.

4. Summary

A tethered free-fall glider has been designed to measure turbulence in the ocean mixed layer. The instrument was successfully tested during a cruise on the Scotian Shelf in June 1996. The vehicle attained a 4:1 gliding ratio with the angle of attack close to 0°. The glider typically stabilized its pitch and roll within the first 10 s of each flight. Vehicle speed started at 0.55 m s^{-1} and decreased to 0.45 m s^{-1} over the period of a 300-s flight due to the increase in drag of the tether cable. Microstructure data from a case with moderate wind forcing demonstrated mixing occurring throughout the ocean mixed layer. In a case with very light winds a region of strong mixing at a depth of 12 m is evident in both the temperature and velocity signals. The noise level of the instrument is of the order of 10^{-9} W kg^{-1}. Other towed and submarine-mounted horizontal profiling systems have been able to achieve similar noise levels by isolation-mounting the sensors (e.g., Lueck et al. 1997).

The principal achievement of this instrument design is that it is able to provide quasi-horizontal profiles of microstructure and turbulent shear starting within 2–3 m of the ocean surface. This capability is unique to EPSONDE-Glider and provides a significant improvement over vertical profilers, which typically do not sample in the top 5–8 m of the ocean. This vehicle will serve as a complementary platform to the vertical profiler because it enables us to make dissipation measurements closer to the ocean surface as well as providing more sampling time within the mixed layer during a profile. We are assuming that the turbulent signal is locally isotropic and that the signal that is measured by the microstructure sensors is essentially a vertical profile (although we are sampling quasi-horizontally). One might well expect horizontal variability due to horizontal changes in the rate at which turbulence is produced locally. For example, this variability could be associated with local strong shear from the wave field or Langmuir cells. These questions have not been addressed in this instrument-focused paper. It would be desirable to improve the glide ratio of EPSONDE-Glider to gather more data close to the ocean surface; hence, attempts are being made to reduce the drag of the instrument.

A major problem encountered in operating the vehicle at sea was that under very light wind conditions the ship tends to drift with the current as opposed to drifting with the wind, which makes it difficult to achieve good separation between the glider/tether cable and the ship. This problem could be minimized by considering climatological weather conditions more carefully when planning an experiment with EPSONDE-Glider. It would be advantageous to develop an algorithm to integrate data from the ship's differential global positioning system and ADCP with glider speed direction and depth. This would make it possible to plot ship–glider separation and azimuth in real time to assist in piloting the vehicle.

Subsequent to the 1996 experiment a number of improvements have been made. First, the glider control deck unit software has been upgraded to run natively under Microsoft Windows 95 or NT. Second, the glider control deck unit program and the TattleTale 8 firmware have been modified to allow the elevator and main wing servos to be shut down. In addition, stop limiters for elevator wing have been incorporated to protect the servo control system from damage. These changes were made because the servo systems are susceptible to failure if improperly handled. Third, we have attempted to improve the flight performance of the vehicle by fairing the mounting straps and servo case on the main wing. In addition the lift cable and brackets have been removed from the main wing to improve the flow over the surface of the wing. A rigid lifting bracket is now attached to the vehicle behind the main wing.

A series of tests with EPSONDE-Glider were recently (July 98) carried out on the Defence Research Establishment Atlantic barge in Bedford Basin. Preliminary analysis of results from these tests indicate that the changes to the vehicle streamlining have improved flight performance. With the elevator wing set at angles of 0°, −10°, and −20°, the gliding ratio was measured to be 5.7:1, 5.2:1, and 4.3:1, respectively. The angle of attack ranged from 3° with the elevator at 0° down to 0° with the elevator at −20°. These results represent a significant improvement over the gliding ratio of 4:1 attained in the 1996 experiment and serve to confirm the theoretical estimates.

Acknowledgments. This program was partially funded by the U.S. Office of Naval Research Grant N00014-93-1-0522. The authors would like to thank the following people at the Bedford Institute of Oceanography who contributed to this project: Scott Young, Lisa Clark, Jean-Guy Dessereault, Bob Ryan, Fred Dobson, George Steeves, John Conrod, Mike LaPierre, Jack Horne, Garon Awalt, Glen Morton, Brian Beanlands, Liam Petrie, Murray Scotney, and the crew of the CSS *Parizeau.* The

authors would also like to acknowledge the contributions of Jeff Scrutton and Scott McLean (Satlantic Inc.); Walter Judge, Phil MacAulay, and Elizabeth Gonzalez (Dalhousie University); and Richard Goldsworthy (Defence Research Establishment Atlantic). Thanks also to George Fowler, Dave Ciochetto, and three anonymous reviewers for their comments on the manuscript.

REFERENCES

Anis, A., and J. N. Moum, 1995: Surface wave-turbulence interactions: Scaling $\epsilon(z)$ near the sea surface. *J. Phys. Oceanogr.,* **25,** 2025–2045.

Dhanak, M., and K. Holappa, 1996: An autonomous ocean turbulence measurement platform. *Workshop on Microstructure Sensors in the Ocean.* Mt. Hood, Oregon, 171–174.

Dobson, F. W., S. D. Smith, and R. J. Anderson, 1994: Measuring the relationship between wind stress and sea state in the open ocean in the presence of swell. *Atmos.–Ocean,* **32,** 237–256.

Dommasch, D. O., S. S. Sherby, and T. F. Connolly, 1967: *Airplane Aerodynamics.* 4th ed., Pitman Publishing, 621 pp.

Gargett, A. E., 1975: Horizontal coherence of oceanic temperature structure, *Deep-Sea Res.,* **22,** 767–776.

——, 1976: An investigation of the occurrence of oceanic turbulence with respect to finestructure. *J. Phys. Oceanogr.,* **6,** 139–156.

——, 1982: Turbulence measurements from a submersible. *Deep-Sea Res.,* **29,** 1141–1158.

Grant, H. L., R. W. Stewart, and A. Moilliet, 1962: Turbulence spectra from a tidal channel. *J. Fluid Mech.,* **12,** 241–268.

Greenan, B. J. W., N. S. Oakey, S. W. Young, L. D. Clark, and J. G. Dessureault, 1997: A tethered free-fall glider to measure ocean turbulence. *Can. Tech. Rep. Hydrogr. Ocean. Sci.,* **186,** vii + 193 pp.

Gregg, M. C., 1980: Microstructure patches in the thermocline, *J. Phys. Oceanogr.,* **10,** 915–943.

Kawaguchi, K., T. Ura, Y. Tomoda, and H. Kobayashi, 1993: Development and sea trials of a shuttle-type AUV ''ALBAC.'' *Proc. Eighth Int. Symp. Unmanned Untethered Submersible Technology.* Portsmouth, NH, Autonomous Undersea Systems Institute.

Levine, E. R., and R. G. Lueck, 1996: Turbulence measurement from an autonomous underwater vehicle. *Workshop on Microstructure Sensors in the Ocean.* Mt. Hood, Oregon, 183–190.

Lueck, R. G., 1987: Microstructure measurements in a thermohaline staircase. *Deep-Sea Res.,* **34,** 1677–1688.

——, D. Huang, D. Newman, and J. Box, 1997: Turbulence measurement with a moored instrument. *J. Atmos. Oceanic Technol.,* **14,** 143–161.

Oakey, N. S., 1977: OCTUPROBE III: An instrument to measure oceanic turbulence and microstructure. Bedford Institute of Oceanography Report Series, BI-R-77-3, 52 pp.

——, 1985: Statistics of mixing in the upper ocean during JASIN Phase 2. *J. Phys. Oceanogr.,* **15,** 1662–1675.

——, 1988: EPSONDE: An instrument to measure turbulence in the deep ocean. *IEEE J. Ocean. Engineer.,* **13,** 124–128.

——, and J. A. Elliott, 1982: Dissipation within the surface mixed layer. *J. Phys. Oceanogr.,* **12,** 171–185.

Osborn, T. R., 1978: Measurements of energy dissipation adjacent to an island. *J. Geophys. Res.,* **83,** 2939–2957.

——, and W. R. Crawford, 1980: An airfoil probe for measuring turbulent velocity flucuations in water. *Air Sea Interaction Instruments and Methods,* F. Dobson, L. Hasse, and R. Davis, Eds., Plenum, 369–386.

——, and R. G. Lueck, 1985a: Turbulence measurements with a towed body. *J. Atmos. Oceanic Technol.,* **2,** 517–527.

——, and ——, 1985b: Turbulence measurements with a submarine. *J. Phys. Oceanogr.,* **15,** 1502–1520.

——, D. M. Farmer, S. Vagle, S. A. Thorpe, and M. Cure, 1992: Measurements of bubble plumes and turbulence from a submarine. *Atmos.–Ocean,* **30,** 419–440.

Simonetti, P., 1998: Low-cost, endurance ocean profiler. *Sea Technol.,* **39,** 17–21.

Yamazaki, H., R. G. Lueck, and T. Osborn, 1990: A comparison of turbulence data from a submarine and a vertical profiler. *J. Phys. Oceanogr.,* **20,** 1778–1786.